

The Importance of Being Symmetric: Flat Rotation Curves from Exact Axisymmetric Static Vacuum Spacetimes

Antonia Seifert^{1,2} 

¹*Institut für Theoretische Physik, Universität Heidelberg, Philosophenweg 12, D-69120 Heidelberg, Germany*

²*School of Physical and Chemical Sciences — Te Kura Matū, University of Canterbury, Private Bag 4800, Christchurch 8140, New Zealand*

Accepted XXX. Received YYY; in original form ZZZ

ABSTRACT

Starting from the vacuum Einstein Field Equations and a static axisymmetric ansatz, we find two new solutions describing an axisymmetric static vacuum spacetime with cylindrical symmetry: One of this exhibits an additional symmetry in z -direction and the other has z -coordinate dependent coefficients. In analogy to the Schwarzschild solution, these metrics describe a static vacuum spacetime and apply in similar settings except for the changed symmetry conditions. Analyzing the low-velocity limit corresponding to the Newtonian approximation of the Schwarzschild metric, we find an effective logarithmic potential. This yields flat rotation curves for test particles undergoing rotational motion within the spacetime described by the line elements, in contrast to Newtonian rotation curves. This analysis highlights how important the symmetry assumptions are for deriving general relativistic solutions.

One example of physical objects that are generally described in the static vacuum low-velocity limit (reducing to Newtonian gravity in the spherically symmetric case) and exhibit axial symmetry are disk galaxies. We show that symmetries and appropriate line elements that respect them are crucial to consider in such settings. In particular, the solutions presented here result in flat rotation curves without any need for dark matter. While these exact solutions are limited to static vacuum spacetimes, their application to physical galaxies relies on appropriate approximations. Nonetheless, they offer valuable insights into explanations for flat rotation curves in galaxies and their implications for dark matter.

Key words: gravitation – galaxies: general – dark matter

1 INTRODUCTION

General relativity (GR) has proven to be a very successful theory of gravity ever since its introduction (Einstein 1915), explaining and predicting phenomena such as Mercury’s perihelion shift (Clemence 1947), black holes (Schwarzschild 1916; Kerr 1963; GRAVITY Collaboration et al. 2018), gravitational waves (Abbott et al. 2016) and providing the foundation of the standard model of cosmology.

To derive the geometry of a given spacetime manifold from the Einstein field equations, it is crucial to impose symmetries on the ansatz for the metric. Examples for such spacetime manifolds are the Schwarzschild solution (Schwarzschild 1916) which is spherically symmetric and static, and the Kerr metric (Kerr 1963) which is axisymmetric and stationary. Both of these solutions are vacuum solutions, i.e. they describe spacetimes without any mass content in the domain of definition. Although the Schwarzschild solution is built on the unphysical assumptions to have a static vacuum spacetime, it reduces to Newtonian gravity in the low-velocity and weak-field limit.

Situations where this limit is applicable, such as in galaxies, are generally assumed to be described by Newtonian gravity. When only considering baryonic matter, the Newtonian prediction fails to explain the rotation curves observed in galaxies (for a review see Bertone & Hooper 2018). This contradiction is commonly resolved by considering a halo of dark matter that contributes to the dynamics

in the galaxy by gravitational interaction only. However, particles constituting this dark matter halo have not been found to date and the nature of dark matter remains an open question in modern physics (for a review see Bertone & Tait 2018). Other approaches to explain the “missing mass” are the theories of modified Newtonian dynamics (MOND, see e.g., Milgrom 1983; McGaugh et al. 2016) and contributions of general relativistic self-interaction effects (GR-SI, see e.g., Deur 2009; Deur et al. 2020). While the latter does not rely on a specific metric, multiple attempts towards a full relativistic treatment of galaxies have been made in the past years (for a review see Re & Galoppo 2024), both from an analytical perspective and by comparison to observations (e.g., Cooperstock & Tieu 2005; Crosta et al. 2020). Lately, Beordo et al. (2024) investigated the applicability of a stationary and axisymmetric class of general relativistic solutions to the Milky Way and found that general relativistic effects can contribute substantially to the rotation curve. However, their class of solutions is based on a stationary metric allowing for frame-dragging effects (see e.g., Astesiano et al. 2022; Stephani et al. 2003) which require further investigation. In this work, we consider *static* metrics instead and analyse their low-velocity limit. This is completely analogous to how the Newtonian approximation emerges from the static spherically symmetric vacuum solution given by the Schwarzschild metric, except for the different symmetry conditions.

In this way, we investigate the implications of the symmetries on

the metric found from the Einstein field equations by analysing static vacuum spacetimes derived under different symmetry assumptions. The Einstein field equations adapted to these conditions are derived in Section 2. The line element emerging from the metric being independent of the z -coordinate is presented in Section 3, together with a second line element that allows for z -dependencies in the coefficients. We then evaluate these line elements in the low-velocity limit and compare them to Newtonian gravity that emerges from the static spherically symmetric vacuum spacetime in the same limit. The findings from this comparison and the applicability of the line elements are discussed in Section 4 before we conclude in Section 5.

2 ANSATZ

To derive the line elements, we choose an ansatz for the metric by considering a suitable foliation of the spacetime manifold that reflects the assumed symmetries. This corresponds to a choice of coordinates that leads to the ansatz in Eq. (2). Intuitively speaking, the coordinates should not mix spatial and time components (staticity) and we want to consider cylindrical coordinates on the spatial part of the manifold. However, as we are working on an arbitrary manifold rather than in Euclidean space, we have to define these coordinates carefully from the Killing vectors reflecting continuous symmetries of the spacetime and submanifolds invariant under the isometry group.

In particular, given a static (and thus also stationary) situation, the manifold M can be foliated as $\mathbb{R} \times \Sigma$ due to the Frobenius condition (e.g., Bartelmann 2019, Section 8.2). We define the time coordinate t such that the Killing vector associated with the symmetry imposed by stationarity is given by ∂_t . Then, by the Frobenius condition, staticity causes the g_{0i} components of the metric to vanish. Furthermore, axial symmetry implies the foliation of Σ into $\Sigma = I_z \times \Pi$ for $I_z \subset \mathbb{R}$ and a radially symmetric two-dimensional section Π . The radial symmetry yields a Killing vector ∂_φ and implies that the group of rotations in two dimensions, $SO(2)$, is an isometry group of the metric on Π . The orbits of this isometry group foliate Π into invariant one-spheres, and we can thus define a radial coordinate ρ such that the circumference of these one-spheres is given by $U = 2\pi\rho$. With this choice of coordinates, we obtain the full foliation

$$M = \mathbb{R} \times I_z \times I_\rho \times \mathbb{S} \quad (1)$$

for $I_\rho \subset \mathbb{R}^+$ and the one-sphere \mathbb{S} , hence the metric is diagonal in the cylindrical coordinates (t, z, ρ, φ) . Thus, we start with the ansatz for the metric given by

$$ds^2 = -e^{2a(\rho,z)} dt^2 + e^{2b(\rho,z)} d\rho^2 + e^{2f(\rho,z)} \rho^2 d\varphi^2 + e^{2h(\rho,z)} dz^2. \quad (2)$$

The exponentials ensure that the prefactors are positive. To parametrise the spacetime using cylindrical coordinates, we can furthermore enforce $b = f$.

The vacuum Einstein field equations thus yield differential equations for the coefficients or equivalently for their exponents. To obtain these, we follow the Cartan formalism (Bartelmann 2019, Section 8.1) and define a dual tetrad

$$\theta^0 = e^a dt, \quad \theta^1 = e^b d\rho, \quad \theta^2 = e^b \rho d\varphi, \quad \theta^3 = e^h dz, \quad (3)$$

such that $ds^2 = \eta_{\mu\nu} \theta^\mu \theta^\nu$ for $\eta_{\mu\nu} = \text{diag}(-1, 1, 1, 1)$ the Minkowski metric. Next, we can determine the connection 1-forms, $\omega^\mu{}_\nu = \Gamma^\mu{}_{\alpha\nu} dx^\alpha$, that relate to the Christoffel symbols, and the curvature 2-forms, $\Omega^\mu{}_\nu = R^\mu{}_{\nu\alpha\beta} \theta^\alpha \wedge \theta^\beta$, corresponding to the Riemann tensor.

This is done using Cartan's structure equations (Cartan 1923) for the torsion-free Levi-Civita connection (i.e. torsion 2-forms $\Theta^\mu = 0$),

$$0 = \Theta^\mu = d\theta^\mu + \omega^\mu{}_\nu \wedge \theta^\nu, \quad (4)$$

$$\Omega^\mu{}_\nu = d\omega^\mu{}_\nu + \omega^\mu{}_\lambda \wedge \omega^\lambda{}_\nu. \quad (5)$$

The tetrad given in Eq. (3) yields the connection forms

$$\omega^0{}_1 = a_{,\rho} e^{-b} \theta^0 = \omega^1{}_0, \quad (6)$$

$$\omega^0{}_3 = a_{,z} e^{-h} \theta^0 = \omega^3{}_0, \quad (7)$$

$$\omega^1{}_3 = b_{,z} e^{-h} \theta^1 - h_{,\rho} e^{-b} \theta^3 = -\omega^3{}_1, \quad (8)$$

$$\omega^2{}_1 = \left(b_{,\rho} + \frac{1}{\rho}\right) e^{-b} \theta^2 = -\omega^1{}_2, \quad (9)$$

$$\omega^2{}_3 = f_{,z} e^{-h} \theta^2 = -\omega^3{}_2, \quad (10)$$

and all other $\omega^\mu{}_\nu$ vanish. Here, $_{,x}$ is used as a short-hand notation for partial derivatives with respect to the variable x . With these, one can obtain the components of the curvature forms:

$$\Omega^0{}_1(e_1, e_0) = e^{-2b} (a_{,\rho\rho} - a_{,\rho} b_{,\rho} + a_{,\rho}^2) + a_{,z} b_{,z} e^{-2h}, \quad (11)$$

$$\Omega^0{}_1(e_3, e_0) = e^{-h-b} (a_{,\rho z} - a_{,\rho} b_{,z} + a_{,\rho} a_{,z} - a_{,z} h_{,\rho}), \quad (12)$$

$$\Omega^0{}_3(e_3, e_0) = e^{-2h} (a_{,zz} - a_{,z} h_{,z} + a_{,z}^2) + a_{,\rho} h_{,\rho} e^{-2b}, \quad (13)$$

$$\Omega^0{}_3(e_1, e_0) = e^{-h-b} (a_{,z\rho} - a_{,z} h_{,\rho} + a_{,z} a_{,\rho} - a_{,\rho} b_{,z}), \quad (14)$$

$$\Omega^2{}_1(e_1, e_2) = e^{-2b} \left(b_{,\rho\rho} + \frac{b_{,\rho}}{\rho}\right) + b_{,z} f_{,z} e^{-2h}, \quad (15)$$

$$\Omega^2{}_1(e_3, e_2) = e^{-h-b} (b_{,\rho z} - b_{,z} h_{,\rho}), \quad (16)$$

$$\Omega^1{}_3(e_3, e_1) = e^{-2h} (b_{,zz} - b_{,z} h_{,z} + b_{,z}^2) + e^{-2b} (h_{,\rho\rho} - b_{,\rho} h_{,\rho} + h_{,\rho}^2), \quad (17)$$

$$\Omega^0{}_2(e_0, e_2) = -\left(a_{,\rho} \left(b_{,\rho} + \frac{1}{\rho}\right) e^{-2b} + a_{,z} b_{,z} e^{-2h}\right), \quad (18)$$

$$\Omega^2{}_3(e_1, e_2) = e^{-h-b} (b_{,z\rho} - b_{,z} h_{,\rho}), \quad (19)$$

$$\Omega^2{}_3(e_3, e_2) = e^{-2h} (b_{,zz} - b_{,z} h_{,z} + b_{,z}^2) + h_{,\rho} \left(b_{,\rho} + \frac{1}{\rho}\right) e^{-2b}. \quad (20)$$

From these components, we find the differential equations for a, b, h ,

$$0 = G_{00} = -e^{-2b} \left(b_{,\rho\rho} + \frac{b_{,\rho}}{\rho} + \frac{h_{,\rho}}{\rho} + h_{,\rho\rho} + h_{,\rho}^2\right) - e^{-2h} (3b_{,z}^2 + 2b_{,zz} - 2b_{,z} h_{,z}), \quad (21)$$

$$0 = G_{11} = e^{-2b} \left(a_{,\rho} b_{,\rho} + \frac{a_{,\rho}}{\rho} + a_{,\rho} h_{,\rho} + h_{,\rho} b_{,\rho} + \frac{h_{,\rho}}{\rho}\right) + e^{-2h} (a_{,z} b_{,z} + a_{,zz} - a_{,z} h_{,z} + a_{,z}^2 + b_{,zz} - b_{,z} h_{,z} + b_{,z}^2), \quad (22)$$

$$0 = G_{22} = e^{-2b} (a_{,\rho\rho} - a_{,\rho} b_{,\rho} + a_{,\rho}^2 + a_{,\rho} h_{,\rho} + h_{,\rho\rho} - b_{,\rho} h_{,\rho} + h_{,\rho}^2) + e^{-2h} (a_{,z} b_{,z} + a_{,zz} - a_{,z} h_{,z} + a_{,z}^2 + b_{,zz} - b_{,z} h_{,z} + b_{,z}^2), \quad (23)$$

$$0 = G_{33} = e^{-2b} \left(a_{,\rho\rho} + a_{,\rho}^2 + \frac{a_{,\rho}}{\rho} + b_{,\rho\rho} + \frac{b_{,\rho}}{\rho}\right) + e^{-2h} (2a_{,z} b_{,z} + b_{,z}^2), \quad (24)$$

$$0 = G_{13} = -e^{-b-h} (a_{,\rho z} - a_{,\rho} b_{,z} + a_{,\rho} a_{,z} - a_{,z} h_{,\rho} + b_{,\rho z} - b_{,z} h_{,\rho}), \quad (25)$$

as the components of the curvature forms give those of the Riemann tensor and thus the Ricci tensor and Ricci scalar which combine to the Einstein tensor. We can now solve these equations for different special cases.

3 RESULTS

The differential Eqs. (21) to (25) can be solved in different ways. One solution is given by the Schwarzschild metric in cylindrical coordinates,

$$ds^2 = -\frac{(1-\Phi)^2}{(1+\Phi)^2} c^2 dt^2 + (1+\Phi)^4 (d\rho^2 + \rho^2 d\varphi^2 + dz^2) \quad (26)$$

where $\Phi = \frac{GM}{2c^2\sqrt{\rho^2+z^2}}$, which can be obtained from the Schwarzschild metric in isotropic coordinates (Eddington 1924). This is a static spherically symmetric vacuum solution. In the language of differential geometry, the static and spherically symmetric situation corresponds to three Killing vectors ∂_t , ∂_φ and ∂_θ .

In this paper, we present two different static cylindrical solutions. The first one considers the Killing vector ∂_z instead of ∂_θ and thus does not have z -dependencies in the coefficients. It is named the *cylinder solution* and derived in Section 3.1. Lifting the condition of z -independence by varying the constants with respect to z (Section 3.2) yields the *disk solution*. In Section 3.3 we discuss the integration constants and scales arising from the solution and in Section 3.4 we consider the trajectories of test particles in the cylinder and disk spacetimes.

3.1 Cylinder Solution

For the z -independent solution to the Einstein field equations, we consider

$$a_{,z} = b_{,z} = h_{,z} = 0. \quad (27)$$

From Eqs. (21) to (25), we thus obtain the four independent differential equations

$$0 = a_{,\rho} b_{,\rho} + \frac{a_{,\rho}}{\rho} + a_{,\rho} h_{,\rho} + h_{,\rho} b_{,\rho} + \frac{h_{,\rho}}{\rho}, \quad (28)$$

$$0 = \frac{a_{,\rho}}{\rho} + 2a_{,\rho} h_{,\rho} + \frac{h_{,\rho}}{\rho} + a_{,\rho\rho} + a_{,\rho}^2 + h_{,\rho\rho} + h_{,\rho}^2, \quad (29)$$

$$0 = b_{,\rho\rho} + \frac{b_{,\rho}}{\rho} + \left(\frac{h_{,\rho}}{\rho} + h_{,\rho\rho} + h_{,\rho}^2 \right), \quad (30)$$

$$0 = b_{,\rho\rho} + \frac{b_{,\rho}}{\rho} + \left(\frac{a_{,\rho}}{\rho} + a_{,\rho\rho} + a_{,\rho}^2 \right), \quad (31)$$

where Eq. (29) follows from the sum of Eqs. (22) and (23). Considering the special case $a_{,\rho} = h_{,\rho}$, i.e.

$$h = a + \frac{1}{2} \ln E \quad (32)$$

for a suitable constant E , Eqs. (28) to (31) reduce to

$$0 = 2a_{,\rho} b_{,\rho} + 2\frac{a_{,\rho}}{\rho} + a_{,\rho}^2, \quad (33)$$

$$0 = 2\frac{a_{,\rho}}{\rho} + 4a_{,\rho}^2 + 2a_{,\rho\rho}, \quad (34)$$

$$0 = b_{,\rho\rho} + \frac{b_{,\rho}}{\rho} - a_{,\rho}^2, \quad (35)$$

combining Eqs. (31) and (34) to obtain Eq. (35). By separation of variables and integration we find that Eqs. (33) to (35) are solved by

$$a = \frac{1}{2} \ln(C \ln \rho + D), \quad (36)$$

$$b = -\frac{1}{4} \ln(C \ln \rho + D) - \ln \rho + \frac{1}{2} \ln B \quad (37)$$

for C, D and B constant. Hence, the z -independent static cylindrical line element

$$ds^2 = -(C \ln \rho + D) c^2 dt^2 + \frac{B}{\rho^2 \sqrt{C \ln \rho + D}} (d\rho^2 + \rho^2 d\varphi^2) + E(C \ln \rho + D) dz^2 \quad (38)$$

with constants B, C, D, E solves the vacuum Einstein field equations in their form given by Eqs. (21) to (25).

3.2 Disk Solution

Starting from the cylinder line element Eq. (38) or equivalently

$$ds^2 = -\left(C \ln \frac{\rho}{R}\right) c^2 dt^2 + \frac{1}{\rho^2 \sqrt{\tilde{C} \ln \frac{\rho}{R}}} (d\rho^2 + \rho^2 d\varphi^2) + E \left(C \ln \frac{\rho}{R}\right) dz^2 \quad (39)$$

for $D = -C \ln R$ with R another constant and defining $\tilde{C} = \frac{C}{B^2}$, we can introduce z -dependencies by varying the constants R, C, E, \tilde{C} with respect to z . The line element Eq. (39) solves Eqs. (28) to (31) both with or without z -dependence in the constants. Thus, combining Eqs. (28) to (31) with the Einstein field equations in Eqs. (21) to (25) we obtain

$$0 = 3b_{,z}^2 + 2b_{,zz} - 2b_{,z} h_{,z}, \quad (40)$$

$$0 = a_{,z} b_{,z} + a_{,zz} - a_{,z} h_{,z} + a_{,z}^2 + b_{,zz} - b_{,z} h_{,z} + b_{,z}^2, \quad (41)$$

$$0 = a_{,z} b_{,z} + a_{,zz} - a_{,z} h_{,z} + a_{,z}^2 + b_{,zz} - b_{,z} h_{,z} + b_{,z}^2, \quad (42)$$

$$0 = 2a_{,z} b_{,z} + b_{,z}^2, \quad (43)$$

$$0 = a_{,\rho z} - a_{,\rho} b_{,z} + a_{,\rho} a_{,z} - a_{,z} h_{,\rho} + b_{,\rho z} - b_{,z} h_{,\rho} \quad (44)$$

to be solved by the (z -dependent) coefficients in Eq. (39). Furthermore, these coefficients also solve Eq. (33) and thus

$$a_{,\rho} = -2b_{,\rho} - \frac{2}{\rho} \quad (45)$$

which together with $a_{,\rho} = h_{,\rho}$ reduces Eq. (44) to

$$0 = -b_{,\rho z} + 4b_{,\rho} b_{,z} + \frac{4b_{,z}}{\rho}. \quad (46)$$

For b given by Eq. (37) with z -dependent R and $\tilde{C} = \frac{C}{B^2}$, this implies

$$0 = \frac{1}{4\rho R} \frac{1}{\ln^2 \frac{\rho}{R}} R_{,z} + \frac{4\left(\tilde{C}_{,z} \ln \frac{\rho}{R} - \frac{\tilde{C} R_{,z}}{R}\right)}{16\rho \tilde{C} \ln \frac{\rho}{R}} \left(\frac{1}{\ln \frac{\rho}{R}} + 1 \right) - \frac{4\left(\tilde{C}_{,z} \ln \frac{\rho}{R} - \frac{\tilde{C} R_{,z}}{R}\right)}{16\rho \tilde{C} \ln \frac{\rho}{R}} \quad (47)$$

$$= \frac{\tilde{C}_{,z}}{4\rho \tilde{C}} \frac{1}{\ln \frac{\rho}{R}} \quad (48)$$

and thus $\tilde{C}_{,z} = 0$.

Let us now assume $b_{,z} \neq 0$, which by $\tilde{C}_{,z} = 0$ implies $R_{,z} \neq 0$. Then, Eq. (43) implies $b_{,z} = -2a_{,z}$ and by varying the constant E in

the h function given in Eq. (32), we find $h_{,z} = a_{,z} + \frac{E_{,z}}{2E}$. Inserting this into Eq. (40), we obtain

$$0 = \left(4b_{,z} + 2\frac{b_{,zz}}{b_{,z}} \right) b_{,z} - \frac{E_{,z}}{E} b_{,z}, \quad (49)$$

$$= \left(\frac{1}{R} \frac{1}{\ln \frac{\rho}{R}} R_{,z} - \frac{2R_{,z}}{R} + \frac{2R_{,zz}}{R_{,z}} + \frac{2R_{,z}}{R \ln \frac{\rho}{R}} \right) b_{,z} - \frac{E_{,z}}{E} b_{,z}. \quad (50)$$

As both R and E are independent of ρ , this is only possible for $b_{,z} = 0$ which contradicts the assumption. We conclude that $b_{,z} = 0$ and as $\tilde{C}_{,z} = 0$, this implies $R_{,z} = 0$. However, note that with these conclusions $E_{,z}$ does *not* have to vanish for the above equation to be fulfilled.

As we have shown that $b_{,z} = 0$ and using $a_{,\rho} = h_{,\rho}$ from Section 3.1, Eqs. (40) to (44) reduce to

$$0 = a_{,zz} - a_{,z} h_{,z} + a_{,z}^2, \quad (51)$$

$$0 = a_{,\rho z}. \quad (52)$$

Thus, additional terms added to Eq. (36) can depend on z . Such terms then correspond to factors $\epsilon(z)$ in the coefficient e^{2a} , i.e. $e^{2a} = e^{2a}|_{\text{cyl.}} \epsilon(z)$ where the subscript cyl. refers to the corresponding term in the cylinder solution which is independent of z . The z -dependence in the h function follows from Eq. (51) which is solved by

$$h = a + \ln a_{,z} + \frac{1}{2} \ln(4\gamma), \quad (53)$$

$$e^{2h} = 4\gamma a_{,z}^2 e^{2a} = \gamma \frac{\epsilon_{,z}^2}{\epsilon} e^{2a}|_{\text{cyl.}} \quad (54)$$

for constant γ using $(e^{2a})_{,z} = e^{2a}|_{\text{cyl.}} \epsilon_{,z} = 2a_{,z} e^{2a} = 2a_{,z} e^{2a}|_{\text{cyl.}} \epsilon$. This results in the z -dependent line element

$$ds^2 = -\epsilon \left(C \ln \frac{\rho}{R} \right) c^2 dt^2 + \frac{\beta}{\rho^2 \sqrt{C \ln \frac{\rho}{R}}} (d\rho^2 + \rho^2 d\varphi^2) + \gamma \epsilon_{,z}^2 \epsilon^{-1} \left(C \ln \frac{\rho}{R} \right) dz^2 \quad (55)$$

for a z -dependent function ϵ and constants β, γ, C, R .

3.3 Scales

In deriving the line elements from the differential Eqs. (21) to (25), several integration constants arise. They can be interpreted as scales for different coordinates in the following way.

In the z -independent line element Eq. (39), the z -coordinate only enters in the differential dz , thus we can choose the scale of the z -coordinate such that $E = 1$. For a physical interpretation of the constant B , we define the radial transition scale ρ_{tr} at which the metric is (locally) spherically symmetric instead of the cylindrical symmetry. At this scale, the coefficients of the spatial part of the metric must be the same:

$$\frac{B}{\rho_{\text{tr}}^2 \sqrt{C \ln \frac{\rho_{\text{tr}}}{R}}} \stackrel{!}{=} C \ln \frac{\rho_{\text{tr}}}{R}, \quad (56)$$

$$B = \rho_{\text{tr}}^2 \left(C \ln \frac{\rho_{\text{tr}}}{R} \right)^{\frac{3}{2}}. \quad (57)$$

The resulting line element for the cylinder solution is thus given by

$$ds^2 = C \left[-\ln \frac{\rho}{R} c^2 dt^2 + \frac{\rho_{\text{tr}}^2}{\rho^2} \sqrt{\frac{\ln^3 \frac{\rho_{\text{tr}}}{R}}{\ln \frac{\rho}{R}}} (d\rho^2 + \rho^2 d\varphi^2) + \ln \frac{\rho}{R} dz^2 \right]. \quad (58)$$

	Cylinder, Eq. (58)	Schwarzschild	Newtonian
by integration	C, D, B	$m = \frac{MG}{c^2}$	
count of scales	3 scales	1 scale	1 scale
interpretation	M, R, ρ_{tr}	$R_S = 2m$	M

Table 1. Relevant scales in the different line elements that arise from solving the differential equations, and how they are interpreted physically. The z -dependent disk line element Eq. (55) would involve an additional transition scale in z -direction relating to the ϵ function.

In this way, the description of the cylinder spacetime depends on two length scales and a conformal factor C (Table 1) that depend on the object described by this spacetime manifold. To analyze the disk solution Eq. (55) in a similar way, we have to fix the function $\epsilon(z)$ first. By considering the effective potential Eq. (64), this can then be related to the mass of the galaxy. The constant R remains unchanged but in addition to the radial transition scale ρ_{tr} we can define a second transition scale z_{tr} determined by $-g_{00}(z_{\text{tr}}) = g_{33}(z_{\text{tr}})$ as the z -coordinate enters the line element explicitly. In total, the disk solution is thus described by four scales.

Comparing our line elements to the Schwarzschild solution, we find interesting similarities. The Schwarzschild line element has a coordinate singularity at the Schwarzschild radius, $r = R_S$. Similarly, the cylinder and disk solutions possess a coordinate singularity¹ for $\rho = R$. These singularities can be interpreted as horizons beyond which a distant observer is not able to see. Furthermore, in the Schwarzschild solution, conformal rescaling of the metric corresponds to the description of a black hole with different mass (Schäfer 2022, Section F.3). In the cylinder line element Eq. (58), the constant C enters as a conformal prefactor. This suggests that the factor C can be interpreted in terms of the mass of the object. In the following section, we will discuss this further by comparison to observations.

3.4 Motion of Particles

For comparing with observations, we consider test particles in the low-velocity limit moving within the spacetimes derived in Section 3.

In this limit, $dx^i \ll c dt = dx^0$, i.e.

$$-c^2 d\tau^2 = ds^2 \approx -e^{2a} c^2 dt^2, \quad (59)$$

$$\frac{dx^i}{c d\tau} \ll \frac{dx^0}{c d\tau} \approx e^{-a} \quad (60)$$

for τ being the proper time. Hence, the geodesic equation

$$\frac{d^2 x^k}{c^2 d\tau^2} = -\Gamma^k_{\mu\nu} \frac{dx^\mu}{c d\tau} \frac{dx^\nu}{c d\tau} \quad (61)$$

reduces to

$$\frac{d^2 x^k}{d\tau^2} \approx e^{2a} \frac{d^2 x^k}{d\tau^2} \approx -c^2 e^{2a} \Gamma^k_{00} (e^{-a})^2 = \frac{c^2}{2} \partial^k g_{00} = -\partial^k \phi \quad (62)$$

for an effective potential $\phi = -\frac{c^2}{2} g_{00} + \text{const.}$ and can thus be compared to the classical equation of motion. In the case of the static spherically symmetric Schwarzschild line element Eq. (26) with small potential Φ , we find

$$ds^2 = (-1 + 4\Phi) c^2 dt^2 + (1 + 4\Phi) (d\rho^2 + \rho^2 d\varphi^2 + dz^2) \quad (63)$$

¹ It is not shown yet whether this coordinate singularity is due to a spacetime singularity or whether it arises from the choice of coordinates only. In analogy to the Schwarzschild horizon, it can probably be avoided by changing the coordinates, but further investigation is needed to find a suitable set of coordinates where this can be shown.

Choice	Result
static spacetime	no g_{0i} components in the metric
spatial foliation, Eq. (1)	diagonal metric, Eq. (2)
cylindrical symmetry	$b = f$ $\Omega^\mu{}_\nu$ and Riemann tensor
vacuum spacetime	Einstein Field Eqs. (21) to (25)
no z -dependence; and $a_\rho = h_\rho$	line element Eq. (39)
variation of constants w.r.t. z	line element Eq. (55)
rescaling of the z -coordinate	$E = 1$
spherically symmetric at ρ_{tr}	constant B , Eq. (57)
	line element Eq. (58)
galactic disk of visible matter, bTFR	constant C , Eq. (71)
	line element Eq. (72)

Table 2. Overview of the assumptions and parametrizations together with their intermediate results along the derivation of the line elements. The choice considering baryonic Tully-Fisher-Relation (bTFR) refers to fixing the constants to match this empirical relation (cf. Section 3.4).

in this limit (Bartelmann 2019, Section 4.3) and thus the effective potential $\phi = -2c^2\Phi = -\frac{GM}{\sqrt{\rho^2+z^2}}$ resembles the Newtonian potential.

Starting from the static cylindrical solutions given by Eqs. (39) and (55) instead, we find the effective potential

$$\phi = A \ln \frac{\rho}{R}, \quad A = \begin{cases} \frac{Cc^2}{2} & z\text{-independent solution, Eq. (39)} \\ \frac{\epsilon Cc^2}{2} & z\text{-dependent solution, Eq. (55)} \end{cases} \quad (64)$$

and thus the equation of motion reads

$$\ddot{\vec{x}} = -\nabla\phi = -\frac{A}{\rho}\mathbf{e}_\rho - \frac{\partial A}{\partial z} \ln \frac{\rho}{R} \mathbf{e}_z. \quad (65)$$

For rotational motion with $z = \text{const.}$, as it is the case for the cylinder solution, we then obtain

$$F_{\text{central}} = \frac{mv^2}{\rho} \stackrel{!}{=} m \frac{A}{\rho} = F_{\text{grav}} = mg, \quad (66)$$

$$v = \sqrt{g\rho} = \sqrt{A}. \quad (67)$$

The rotational velocity in this case is thus constant with respect to ρ , i.e. it corresponds to flat rotation curves. Note that this will happen for any effective potential of logarithmic form. The logarithmic potential follows directly from the line element in the low-velocity limit without consideration of any particular situation apart from the imposed symmetry conditions. In particular, we find this result both for the cylinder and for the disk solution, the only difference between these in the low-velocity limit is the form of the A factor. This factor will involve the function $\epsilon(z)$ for the disk solution and is constant for the cylinder solution.

Up to this point, the line elements and all considerations in this work are purely theoretical and can be obtained from differential geometry and the respective symmetry assumptions only (Table 2). The constants in the line elements arise from integration constants in the differential equations that can be reformulated in terms of appropriate length scales but are not of any physical value yet.

To apply the line elements as models for physical phenomena, we have to compare them to observations and use this to fix the constants. We thus need to consider a situation of cylindrically distributed matter. A prime example of this is the visible matter in a galaxy. Assume an observer within the disk to which the main *visible* mass content appears to be located at the centre of the galaxy and the mass distributed across the surrounding disk is negligible compared to this central mass. If we do *not* consider any dark matter halo but only visible baryonic matter, the cylinder line element applies. The scales discussed in Section 3.3 can be interpreted as the horizon R

with the main mass content located at radii $\rho < R$, and the length scale ρ_{tr} constructed such that the line element is locally spherically symmetric. By Eq. (67), we obtain flat rotation curves in the low-velocity limit without involving any dark matter.

Another relation that applies in this context and that can thus be used to constrain the constants is the baryonic Tully-Fisher relation (bTFR, Tully & Fisher 1977). This empirical relation states that the asymptotic velocity V_∞ , i.e. the rotational velocity approached for $\rho \rightarrow \infty$ by the observed flat rotation curve of a disk galaxy, and its baryonic mass M are related by the power-law

$$V_\infty^\kappa \propto M \quad (68)$$

$$\left(\frac{V_\infty}{c}\right)^\kappa = \frac{\mu}{4} GM \quad (69)$$

for a phenomenologically defined proportionality constant μ and exponent $\kappa \approx 4$. The relation is commonly assumed to be sustained by the dark matter halo. However, as we do not need dark matter to explain flat rotation curves in the disk and cylinder spacetimes, we consider the bTFR due to the baryonic matter only in these spacetimes and without any dark matter. In the regime far from the centre of mass but within the disk of the galaxy, the cylinder solution applies. Thus, we find

$$v = V_\infty = \frac{c}{\sqrt{2}} \sqrt[4]{\mu GM} \quad (70)$$

from Eq. (67) and can hence constrain the constant C of the line element Eq. (39) using Eq. (64),

$$C = \frac{2A}{c^2} = \frac{2}{c^2} v^2 = \sqrt{\mu GM} = \sqrt{\frac{\tilde{\mu}}{c^2} \frac{GM}{c^2}}. \quad (71)$$

The left-hand side of Eq. (69) is dimensionless and GM is of the dimension of $[L^3T^{-2}]$, thus the dimension of μ is $[L^{-3}T^2]$ and the constant C is dimensionless. As given in Eq. (71), this constant can also be formulated in terms of the acceleration scale $\tilde{\mu} = \mu c^4$, the velocity of light and the length scale $\frac{GM}{c^2} = \frac{R_S}{2}$ related to the Schwarzschild radius R_S . The acceleration scale can then be discussed in comparison to other models explaining flat rotation curves.

Based on the constants defined in this way, the resulting line element reads

$$ds^2 = \sqrt{\mu GM} \left[\ln \frac{\rho}{R} (-c^2 dt^2 + dz^2) + \frac{\rho_{\text{tr}}^2}{\rho^2} \sqrt{\frac{\ln^3 \frac{\rho_{\text{tr}}}{R}}{\ln \frac{\rho}{R}}} (d\rho^2 + \rho^2 d\varphi^2) \right]. \quad (72)$$

4 DISCUSSION

The reconsideration of the vacuum Einstein field equations for a static metric in cylindrical coordinates has revealed new analytic solutions given by the cylinder line element Eq. (72) and the disk line element Eq. (55) with important implications and applications in the description of galaxies and dark matter. The solutions presented here differ from other spacetime metrics due to the symmetry conditions chosen in their derivation. These symmetries are fundamentally imprinted in the solutions and dictate the applicability of the results. At the same time, the substantial changes in the motion of test particles obtained from this analysis prove that the choice of symmetries is crucially important when deriving general relativistic solutions.

4.1 Assumptions and Applicability

The solutions presented here were derived from the same assumptions as the Schwarzschild solution (Schwarzschild 1916) except for

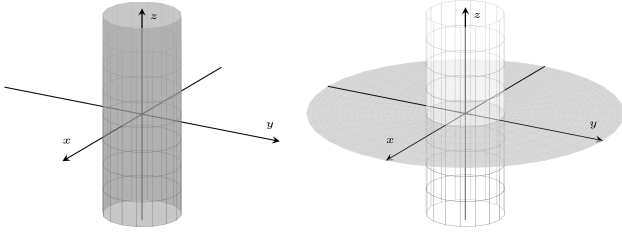


Figure 1. Singularities in the settings described by the line-elements discussed here, the z -independent cylinder solution, Eq. (72), (left) and the z -dependent disk solution, Eq. (55), (right) for an ϵ function singular in $z = 0$ chosen as an example.

the symmetry conditions. In particular, the Schwarzschild solution is spherically symmetric, while the cylinder and disk solutions possess only axial symmetry. However, spherical symmetry also implies axial symmetry, thus the Schwarzschild solution solves the Einstein field equations in their form given in Eqs. (21) to (25). This can be checked in appropriate coordinates using the metric in Eq. (26).

In deriving the cylinder and disk solutions, the axial symmetry was imposed by choosing cylindrical coordinates and enforcing the coefficients e^{2f} and e^{2b} to agree. Multiple solutions in cylindrical coordinates have been derived before (Stephani et al. 2003) but not with this specific choice of coordinates. In particular, for none of the static vacuum solutions presented by Stephani et al. (2003) the coefficients e^{2f} and e^{2b} agree. The choice of coordinates considered in this paper proves particularly useful in the description of galaxies. However, for different settings and for comparison to other solutions, reparameterizing it in different coordinates would be helpful.

Additionally, investigating different coordinate choices is an important tool to understand the singularities in the line elements. Concerning the Schwarzschild solution, the coordinates in Eq. (26) and the Schwarzschild coordinates (Schwarzschild 1916) exhibit two singularities at $r = 0$ and at $r = R_S$ (for $r = \sqrt{\rho^2 + z^2}$), while the Kruskal-Szekeres coordinates are singular at $r = 0$ only (e.g., Misner et al. 1973), thus $r = R_S$ is a coordinate singularity. By analogy, one might suspect that the singularity at $\rho = R$ in the cylinder and disk solutions is a coordinate singularity as well, however, this remains to be proven. It could then be interpreted as a horizon analogous to the Schwarzschild radius, which shields the mass content at the centre of the radial configuration.

Anywhere except for the singularities, the energy-momentum tensor vanishes according to the vacuum Einstein field equations. At the singularities, however, no statement can be made. This suggests for the energy-momentum tensor of the Schwarzschild solution to be of the form $\delta(r)$. Similarly, the energy-momentum tensor of the disk and cylinder solutions can be interpreted to be proportional to $\delta(\rho)$, but its dependence on z is not known. In the line element Eq. (55), the function $\epsilon(z)$ can impose additional conditions on the z coordinates, e.g., the energy-momentum tensor would have to vanish for all $z \neq 0$ if ϵ was singular in $z = 0$ only. Based on the coordinate singularities in the line elements, the latter can be interpreted them to represent the situations shown in Fig. 1. The appearances in the sketches motivate referring to them as the *cylinder solution* and *disk solution* as done throughout the paper.

Both solutions are vacuum solutions, as is the Schwarzschild solution. Although this does not agree with the physical reality, it represents an important limiting case. In situations where the mass content in the environment is negligible compared to the central mass, as it is the case for a black hole, the vacuum solution is an appropriate approximation. Similarly, the cylinder and disk solutions are viable

approximations for a cylindrical configuration where the main mass content is centered at $\rho = 0$ and the mass content in the surroundings is negligible compared to this.

4.2 Importance of Nonlinearities

Apart from the unknown mass configuration in the singularities as a source of spacetime curvature, the nonlinear nature of general relativity also causes curvature to enhance itself, although constrained by the imposed symmetry conditions. This suggests an analogy of the vacuum solution to the pure field case in Quantum Chromodynamics (QCD), as this theory is nonlinear as well. Investigating the Lagrangian as done for the path integral in QCD, we find that for the gravitational field $\psi_{\mu\nu} = g_{\mu\nu} - \eta_{\mu\nu}$, the general relativistic pure-field Lagrangian can be expressed in the polynomial form (see e.g., Zee 2013)

$$\mathcal{L} = \sum_{n=0}^{\infty} (16\pi G M)^{\frac{n}{2}} \psi^n (\partial\psi\partial\psi), \quad (73)$$

where the $n = 1$ term is of order \sqrt{GM} , which supports the finding of $\sqrt{\mu GM}$ as the coefficient of the effective potential in Section 3.4.

Furthermore, the nonlinearities in general relativity cause self-interaction, which will be relevant beyond a certain mass scale. For example, Newtonian gravity is not able to explain Mercury's perihelion shift, but the Schwarzschild solution is needed for this. In this paper, we have shown that the form of the metric and the trajectories of test particles are crucially influenced by the symmetry conditions imposed to derive them. This also affects the mass scales at which general relativistic effects become relevant in systems with cylindrical symmetry, opposed to those with spherical symmetry. For example, galaxies are generally assumed not to be massive enough to exhibit general relativistic effects known for spherically symmetric settings such as black holes. However, considering their axisymmetric configuration without spherical symmetry but differing length scales characterising the ρ - and z -directions, this assumption has to be re-evaluated and general relativistic effects can become relevant.

4.3 Relevant Scales

The different scales of the radial and the z -coordinate motivate that the derivatives with respect to ρ and z in Eqs. (21) to (25) cannot cancel each other and thus the variation of constants is reasonable to obtain the z -dependence in the disk solution. In general, Eqs. (21) to (25) cannot be split into the ρ -dependent Eqs. (28) to (30) and the z -dependent Eqs. (40) to (44). For example, the Schwarzschild metric in cylindrical coordinates does not fulfill the equations involving only one coordinate (Eqs. (28) to (31) and Eqs. (40) to (43)) but satisfies the vacuum Einstein field equations in cylindrical coordinates, Eqs. (21) to (25). Thus, the disk and cylinder line elements are not the only solutions solving the latter set of equations. However, they are the ones relevant to scenarios where the derivatives with respect to different coordinates cannot compensate for each other. In terms of the potential, this means that it scales differently with different coordinates.

In Newtonian gravity, the potential in such symmetry conditions is calculated as done in Appendix A for a line-like source. There, the source at $\rho = 0$ is assumed to be finite and of length $2a$. The disk and cylinder solutions could both describe such a setting, as the energy-momentum tensor and thus the mass density is singular at $\rho = 0$ and not specified further. In the two limits discussed in Appendix A, a logarithmic potential is found for small radii and the inverse-radius

law is recovered in the far-field limit. In a sense, the Newtonian treatment is interpolating between the two effective potentials. It is, however, based on the mass density distribution and only valid for a specific choice of source at $\rho = 0$. In the corresponding generally relativistic situation given by the cylinder solution, this choice of distribution is not the only valid one, as we only assume symmetry conditions and not a specific choice of mass configuration. When interpreting our solutions, we find the mass to be located at the singularities and beyond the horizon, i.e., at $\rho < R$, but no other choices are made.

4.4 Model for Flat Rotation Curves

Recovering Newtonian gravity from the Einstein field equations by assuming vacuum, static, spherically symmetric conditions and the limits of low velocities and $r = \sqrt{\rho^2 + z^2} \gg R_S$ (which corresponds to the small field limit) with the mass assumed to be located at the singularity at $r = 0$, results in an effective potential $\phi = -\frac{GM}{r}$ and effective acceleration proportional to $\frac{1}{r^2}$. In contrast, applying the same conditions as in the derivation of Newtonian gravity except for the symmetry conditions, we find a logarithmic effective potential and accelerations proportional to $\frac{1}{r}$ from the cylinder and disk solutions. The rotational velocities obtained from the Newtonian case differ from the ones observed in Nature. Newtonian gravity is not able to explain the flat rotation curves in galaxies with baryonic matter only which has been one of the reasons to introduce dark matter. Importantly, a logarithmic effective potential as obtained from the cylinder and disk solutions yields flat rotation curves when considering rotational motion in a plane of constant z -coordinate, without any need to introduce dark matter.

People have investigated such potentials and respective accelerations to explain flat rotation curves without the help of dark matter (see [Deur \(2009\)](#); [Deur \(2017\)](#) for an argument based on approximately solving general relativity numerically and then enforcing a cylindrical symmetry, and [Deur et al. \(2020\)](#) for an analysis of the GR-SI approach involving a disk model based on a logarithmic effective potential), but here it emerges exactly and analytically from the vacuum Einstein field equations. The results match observations for appropriately chosen constants (Section 3.4). When fit to the observations, the MOND model (see e.g., [McGaugh et al. 2016](#)) also approaches the acceleration obtained from the logarithmic potential in the limit far from the centre (Fig. 2).

Using the asymptotic velocities from the SPARC catalog ([Lelli et al. 2016](#)), we can fit the baryonic Tully-Fisher relation (Fig. 3) to obtain the constants in the potential and thus in the line element. The parameters from the fit give the exponent, which is within 1σ of the assumption $\kappa = 4$, and the coefficient of the power-law. Expressing the latter in terms of the acceleration scale $\tilde{\mu}$ as given in Eq. (71), we find

$$\tilde{\mu} = (1.1 \pm 0.4) \cdot 10^{-10} \frac{\text{m}}{\text{s}^2} \quad (74)$$

which agrees with the MOND acceleration scale ([McGaugh et al. 2016](#)). However, this approach explains the bTFR better than the pure MOND interpolation function does (see Appendix B). Instead, the MOND acceleration scale is found as a fundamental scale in the cylinder line element that contributes to the coefficient C in Eq. (71) together with the constants c , G and the mass.

In the case of the disk solution, we also find a logarithmic potential and can interpret the integration constants by comparing to observations in a similar way. However, the function $\epsilon(z)$ has to be fixed first. This should be done to recover profiles in z -direction that

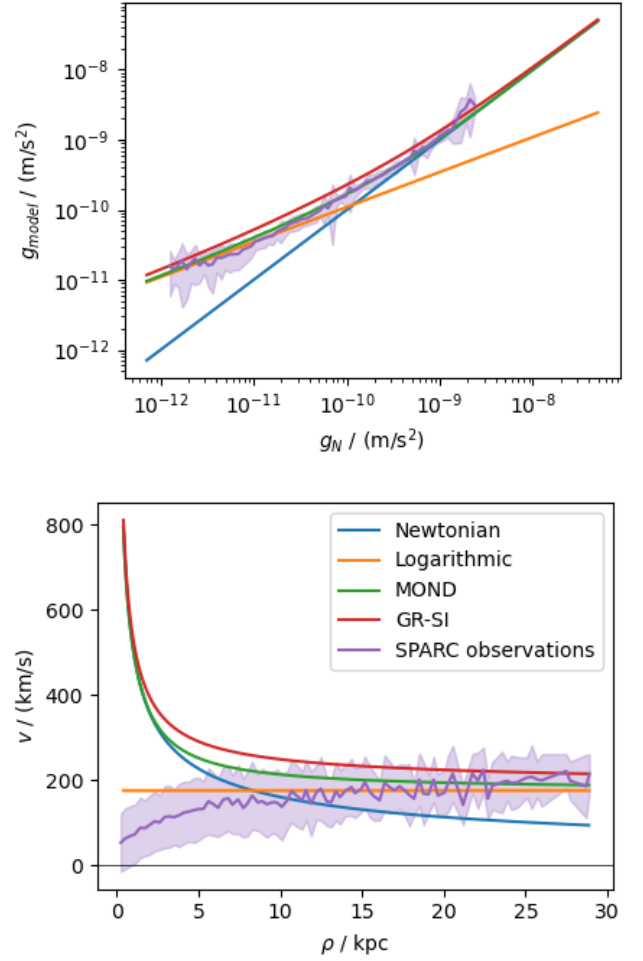


Figure 2. Functional form of the effective acceleration $g_{\text{model}} = |\nabla\phi|$ for arbitrary coefficients plotted as a function of the Newtonian acceleration, g_N , at the respective radius (above) and the corresponding rotation curves, $v = \sqrt{g\rho}$, according to Eq. (67) with ρ the radial coordinate in the $z = 0$ plane (below). The models considered in the plot are the Newtonian potential, the logarithmic potential following from the cylinder and disk solutions, the MOND model by [McGaugh et al. \(2016\)](#) and the GR-SI model by [Deur et al. \(2020\)](#). For comparison, the mean and standard deviation for rotation curves from the SPARC catalog ([Lelli et al. 2016](#)) are shown. Note that the logarithmic potential from the cylinder solution is only applicable beyond the horizon R , thus it is not expected to match observations for low $\rho < R$ and high $g_N > \frac{GM}{R^2}$ values.

are found observationally and requires further investigation. In doing this, ϵ can also be chosen such that the line element Eq. (55) resembles the cylinder solution Eq. (72) for $z \rightarrow 0$ and the potential decays appropriately for $z \rightarrow \infty$.

Importantly, describing the motion of test particles with the effective potentials from Section 3.4 is only possible under certain conditions. First, the physical situation has to obey the symmetry conditions of the metric, i.e., cylindrical symmetry and staticity, at least as a viable approximation. Note that stationarity is not sufficient to apply the metrics derived here. Additionally, the effective potential is derived from a vacuum metric with an energy-momentum tensor proportional to a delta distribution. We can thus only apply this effective potential to situations with negligible mass distributions outside the singularities.

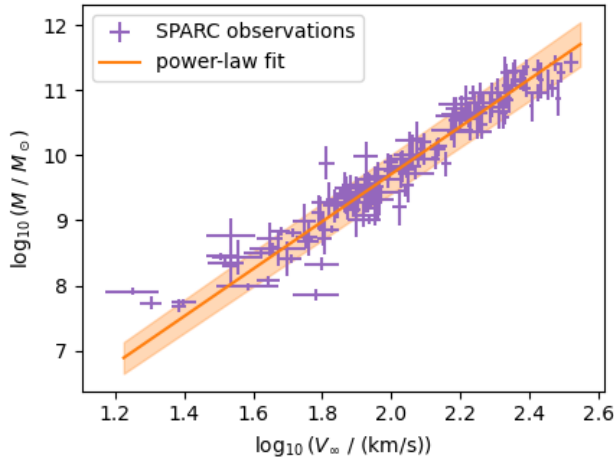


Figure 3. Asymptotic velocities and fit of the power-law for the rotation curves from the SPARC catalog (Lelli et al. 2016). The fit results in $\log_{10} \left(\frac{M}{M_{\odot}} \right) = (3.64 \pm 0.07) \cdot \log_{10} \left(\frac{V_{\infty}}{\text{km/s}} \right) + (2.43 \pm 0.15)$. It is performed based on the mass models by Lelli et al. (2016) and agrees within $1\text{--}2\sigma$ with the fits in their paper.

4.5 Interpretation in the Context of Galaxies

For an approximately static galaxy with negligible mass content outside the horizon R , we can interpret the cylinder solution as the metric of an observer within the galactic plane of non-zero thickness, with a z -coordinate negligible compared to the thickness of the plane. For z differing significantly from zero, intuitively speaking “leaving the plane”, the disk solution becomes a suitable approximation to describe the spacetime in this regime. When moving even further away from it, the symmetry conditions change as the object is of finite size. For $R \ll \rho$, the situation does not appear cylindrically symmetric anymore but spherically symmetric. In this case, the Schwarzschild metric and its Newtonian approximation describe the situation. Note that the Schwarzschild metric is not found as a limiting case neither for the cylinder nor for the disk solution. This is due to the changing symmetry conditions throughout different regimes which is not captured by any of the solutions. The choice of symmetries in the derivation corresponds to particular boundary conditions and is reflected the resulting metric. In particular, the coefficients of the cylinder solution are independent of z which correspond to a different Killing vector. Concerning the disk solution, it can approach a spherical symmetric situation to some extent by choosing the $\epsilon(z)$ function appropriately, but it will not become fully spherically symmetric due to the coordinate singularity at $\rho = R$. To describe the transition to the Schwarzschild and Newtonian line elements, the symmetry conditions and the singularities arising in the derivation of the metrics would have to change from $\rho = R$ close to the object to $r = R_S$ for a distant observer.

As the Einstein field equations are differential equations and derivatives have to be taken locally, *a priori* the solutions are local as well. A full picture of the different regimes will involve multiple local solutions that apply in different regimes, as illustrated in Fig. 4. Combining these results quantitatively to describe the interpolating regimes is a non-trivial task. Important choices towards this are the ϵ function which can be constructed such that it interpolates between the cylinder and the disk solutions, and the scale ρ_{tr} (and z_{tr} for the disk solution). This length scale is defined such that the line element

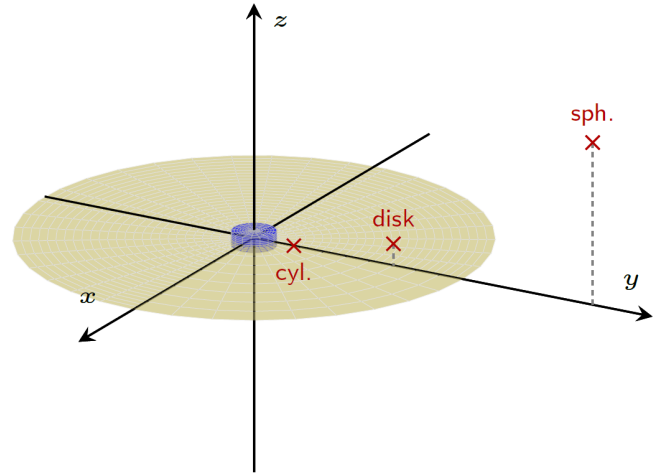


Figure 4. Sketch (not to scale) of the regimes in the environment of a galaxy where the different solutions apply (cylindrical, disk and the spherically symmetric solution from the Schwarzschild/Newtonian case).

is spherically symmetric at $\rho = \rho_{\text{tr}}$. Although this is the case only locally in the cylinder and disk solutions, it can be used to connect the axisymmetric and spherically symmetric line elements. Joining them in this way will, however, not be differentiable in general. Thus, for a full galaxy model, a more involved differentiable metric or at least a different choice of coordinates would be needed. This solution would be an important model in the limiting case of the static vacuum spacetime, i.e. negligible and non-rotating mass distribution outside the horizon. However, lifting the assumptions of staticity to obtain a stationary metric and allowing for a non-vanishing energy-momentum tensor in the Einstein field equations would allow for more physical solutions (Astesiano et al. 2022; Re & Galoppo 2024; Beordo et al. 2024).

The line elements and their applications provide a starting point for investigating the implications of full general relativity on dark matter in galaxies. They show that choosing symmetry conditions adequately is crucial when considering a gravitational system in the general relativity framework. To address the consequences of these results to their full extend, further research is needed. In particular, the regimes of applicability of these line elements and the transition between them (c.f. Fig. 4) have to be investigated carefully. Furthermore, the insights on the importance of symmetries should also be considered in other gravitational systems that cannot be explained with Newtonian gravity. The need for dark matter to explain observed phenomena in gravitational systems has to be re-evaluated carefully based on the individual symmetry conditions of the different systems.

5 CONCLUSIONS

We have solved the vacuum Einstein field equations for a static metric in cylindrical coordinates, resulting in the z -independent cylinder line element Eq. (72) and the z -dependent disk line element Eq. (55). Both of these solutions are important theoretical solutions to the vacuum Einstein field equations.

The derivation of the cylinder line element is done based on the same assumptions as for the Schwarzschild solution (Schwarzschild 1916) except for the symmetries. In particular, the cylinder solution depends on the cylindrical radius ρ only, while the Schwarzschild solution depends on the spherical radius $r = \sqrt{\rho^2 + z^2}$ instead. The

disk line element then follows from the cylinder solution by variation of constants with respect to the z -coordinate. The cylinder and disk solutions are thus applicable under the same conditions as the Schwarzschild solution and its Newtonian approximation, except for the symmetry assumptions. The choice of symmetry conditions can be seen analogously to particular choices of boundary conditions in classical physics. The choices made for the derivation are prominently reflected in the final results. This is the case for symmetry conditions in general relativity as well and gives rise to fundamental differences between the cylinder and disk solutions on the one hand and the spherically symmetric Schwarzschild solution on the other. As a change of symmetries is described by neither of them, they do not approach the same limits but interpolating metrics would be needed.

All of the solutions discussed here describe static vacuum spacetimes. They will thus not yield a full physical model for any object such as galaxies but they represent important limiting cases. In a spherically symmetric setting with a central mass being much larger than a possible additional mass configuration in the environment and for low velocities, the Schwarzschild solution reduces to the Newtonian case. This is used throughout classical mechanics very successfully and even thought to apply in the setting of galaxies. Similarly, the disk and cylinder solutions can be applied as a limiting case when studying objects with substantially high central mass, i.e. negligible mass content in the environment, and cylindrical symmetry. The prime example of such a situation is a disk galaxy, where the cylinder and disk solutions are even more viable than the Schwarzschild and Newtonian line elements.

By considering the motion of particles in different spacetimes in the low-velocity limit, we have shown that the symmetry assumptions fundamentally change the trajectories of test particles. In particular, rotational motion in the cylinder and disk spacetimes yield flat rotation curves while the Schwarzschild solution reduces to Newtonian gravity in this limit.

These flat rotation curves arise naturally from an axially symmetric configuration with significantly differing scales in ρ - and z -directions without further assumptions, only the coefficients have to be fixed by observations. This is done by using the baryonic Tully-Fisher relation in Section 3.4, but the actual form of the constant C in Eq. (58) depends on the observations used. The line elements are applicable to any setting exhibiting cylindrical or at least axisymmetric symmetry, independently of how this configuration may have developed.

For example, the line elements presented here are very successful in explaining the flatness of rotation curves in disk galaxies. They both relate to the GR-SI model (e.g., Deur et al. 2020) which is built upon a logarithmic potential, and yield the MOND acceleration scale (e.g., McGaugh et al. 2016) as a scaling for the force strength when comparing to observations, while not departing from the well-known general relativity framework in any way nor from the low-velocity limit generally considered when describing galaxies. However, it must be kept in mind that the solutions cannot provide a full galaxy model as they are vacuum solutions and rely on the staticity assumption. Instead, they can only relate to the physical settings in appropriate limits and approximations. The investigation of these solutions is thus an important step towards a better understanding of dark matter but cannot be seen as a full explanation of the observationally found galaxy rotation curves yet.

The fact that the symmetries alone change the resulting spacetime metric and the applicability of the cylinder and disk solutions to the description of galaxies in appropriate regimes provide deep insights into the application of general relativity in galaxies. It is crucial to investigate the regimes of applicability of these solutions to understand

its implications to what is typically considered as dark matter. Additionally, the changes in the spacetime arising from the symmetries should be considered in other gravitating systems as well for a better understanding of gravity from general relativity in these situations and how it relates to dark matter.

ACKNOWLEDGEMENTS

I am deeply thankful to Matthias Bartelmann for his supervision and support and to the Astrophysics Group at Old Dominion University, namely Alexandre Deur, Balša Terzić, William Clark and Emerson Rogers, for their comments and discussions on the applications and interpretation of the solutions. Furthermore, I want to thank Adrian Hosak and Frederik Kortkamp for their helpful thoughts and insights over the course of developing this paper.

DATA AVAILABILITY

The theoretical analysis of the metric based on the Einstein field equations is done without any observational constraints from data. For comparison with other models, we considered the SPARC catalog found at <http://astroweb.cwru.edu/SPARC/>.

REFERENCES

- Abbott B. P., et al., 2016, *Phys. Rev. Lett.*, **116**, 061102
- Astesiano D., Cacciatori S. L., Gorini V., Re F., 2022, *The European Physical Journal C*, **82**
- Bartelmann M., 2019, General Relativity. Lecture Notes, Heidelberg University Publishing, doi:10.17885/heup.534, <https://heup.uni-heidelberg.de/catalog/book/534>
- Beordo W., Crosta M., Lattanzi M. G., Re Fiorentin P., Spagna A., 2024, *MNRAS*, **529**, 4681
- Bertone G., Hooper D., 2018, *Reviews of Modern Physics*, **90**, 045002
- Bertone G., Tait T. M. P., 2018, *Nature*, **562**, 51
- Cartan E., 1923, *Annales scientifiques de l'École normale supérieure*, **40**, 325–412
- Clemence G. M., 1947, *Reviews of Modern Physics*, **19**, 361
- Cooperstock F. I., Tieu S., 2005, *arXiv e-prints*, pp astro-ph/0507619
- Crosta M., Giammaria M., Lattanzi M. G., Poggio E., 2020, *MNRAS*, **496**, 2107
- Deur A., 2009, *Phys. Lett. B*, **676**, 21
- Deur A., 2017, *European Physical Journal C*, **77**, 412
- Deur A., Sargent C., Terzić B., 2020, *ApJ*, **896**, 94
- Eddington A., 1924, *The Mathematical Theory of Relativity* (2nd ed.). Cambridge University Press
- Einstein A., 1915, *Sitzungsberichte der Königlich Preussischen Akademie der Wissenschaften*, pp 844–847
- GRAVITY Collaboration et al., 2018, *A&A*, **615**, L15
- Kerr R. P., 1963, *Phys. Rev. Lett.*, **11**, 237
- Lelli F., McGaugh S. S., Schombert J. M., 2016, *AJ*, **152**, 157
- McGaugh S. S., Lelli F., Schombert J. M., 2016, *Phys. Rev. Lett.*, **117**, 201101
- Milgrom M., 1983, *ApJ*, **270**, 365
- Misner C. W., Thorne K. S., Wheeler J. A., 1973, *Gravitation*. Volume I. W. H. Freeman and Company
- Re F., Galoppo M., 2024, *arXiv e-prints*, p. arXiv:2403.03227
- Schwarzschild K., 1916, *Sitzungsberichte der Königlich Preussischen Akademie der Wissenschaften*, pp 189–196
- Schäfer B. M., 2022, General Relativity: Geometric Structure and Dynamics of Spacetime. Lecture Notes, Heidelberg University Publishing, doi:10.17885/heup.1056, <https://heup.uni-heidelberg.de/catalog/book/1056>

Stephani H., Kramer D., MacCallum M., Hoenselaers C., Herlt E., 2003, *Exact Solutions of Einstein's Field Equations*, 2 edn. Cambridge Monographs on Mathematical Physics, Cambridge University Press
 Tully R. B., Fisher J. R., 1977, *A&A*, **54**, 661
 Zee A., 2013, *Einstein Gravity in a Nutshell*. Princeton University Press

APPENDIX A: NEWTONIAN GRAVITY FOR LINE-LIKE SOURCES

For an extended line-like source in Newtonian gravity, i.e. with the density ϱ given by

$$\varrho(\rho, z) \propto \frac{\delta(\rho)}{\rho} \Theta(a+z) \Theta(a-z), \quad (\text{A1})$$

we find

$$\phi(\rho, z) = \int \tilde{\rho} d\tilde{\rho} d\varphi d\tilde{z} \frac{\varrho(\tilde{\rho})}{\sqrt{(\tilde{\rho}-\rho)^2 + (\tilde{z}-z)^2}} \quad (\text{A2})$$

$$\propto 2\pi \int_{-a}^a d\tilde{z} \frac{1}{\sqrt{\rho^2 + (\tilde{z}-z)^2}} \quad (\text{A3})$$

which yields

$$\phi(\rho, 0) \propto \frac{1}{2} \left(-\ln \left(1 - \frac{z'}{\sqrt{\rho^2 + z'^2}} \right) + \ln \left(1 + \frac{z'}{\sqrt{\rho^2 + z'^2}} \right) \right) \Big|_{-a}^a \quad (\text{A4})$$

$$= -\ln \left(1 - \frac{a}{\sqrt{\rho^2 + a^2}} \right) + \ln \left(1 + \frac{a}{\sqrt{\rho^2 + a^2}} \right) \quad (\text{A5})$$

$$= \ln \left(\frac{\rho^2 + a^2 + 2a\sqrt{\rho^2 + a^2} + a^2}{\rho^2 + a^2 - a^2} \right) \quad (\text{A6})$$

$$= \ln \left(1 + 2\frac{a}{\rho} \left(\frac{a}{\rho} + \sqrt{1 + \left(\frac{a}{\rho} \right)^2} \right) \right) \quad (\text{A7})$$

within the disk. Two limits are important when investigating this potential. First, consider $\frac{a}{\rho} \gg 1$, i.e., close to the center of mass at $\rho = 0$, and obtain

$$\phi(\rho, 0) \lesssim \ln \left(4 \frac{a^2}{\rho^2} \right) \quad (\text{A8})$$

$$= -2 \ln \left(\frac{\rho}{2a} \right) \quad (\text{A9})$$

which is of logarithmic form. Conversely, the limit far from the centre, i.e. $\frac{a}{\rho} \ll 1$, yields

$$\phi(\rho, 0) \lesssim \frac{2a}{\rho} \left(\frac{a}{\rho} + \sqrt{1 + \left(\frac{a}{\rho} \right)^2} \right) + \mathcal{O} \left(\left(\frac{a}{\rho} \right)^2 \right) \quad (\text{A10})$$

$$= \frac{2a}{\rho} + \mathcal{O} \left(\left(\frac{a}{\rho} \right)^2 \right) \quad (\text{A11})$$

which reduces to the Newtonian potential.

APPENDIX B: THE BARYONIC TULLY-FISHER RELATION AND THE MOND ACCELERATION SCALE

McGaugh et al. (2016) found the functional form

$$g_{\text{MOND}}(g_{\text{bar}}) = \frac{g_{\text{bar}}}{1 - e^{-\sqrt{\frac{g_{\text{bar}}}{g_{\dagger}}}}} \quad (\text{B1})$$

$$g_{\text{MOND}}(z) = g_{\dagger} \frac{z}{1 - e^{-\sqrt{z}}} \quad (\text{B2})$$

to describe the relation of the observed and the expected baryonic (Newtonian) accelerations based on the MOND acceleration scale $g_{\dagger} = 1.2 \cdot 10^{-10} \frac{\text{m}}{\text{s}^2}$ and $z = \frac{g_{\text{bar}}}{g_{\dagger}}$. In the non-Newtonian limit, $z \ll 1$, this approaches

$$g_{\text{MOND}} \approx g_{\dagger} \sqrt{z} = \sqrt{g_{\dagger} g_{\text{bar}}} \quad (\text{B3})$$

which corresponds to a rotational velocity of

$$\frac{mv^2}{r} = m \sqrt{g_{\dagger} g_{\text{bar}}} \quad (\text{B4})$$

$$v^4 = r^2 g_{\dagger} \frac{GM}{r^2} \quad (\text{B5})$$

$$v^4 = g_{\dagger} GM \quad (\text{B6})$$

using $g_{\text{bar}} = \frac{GM}{r^2}$. In contrast to this, the baryonic Tully-Fisher relation in its form given in Eq. (69) yields

$$v^4 = \frac{\tilde{\mu}}{4} GM \quad (\text{B7})$$

where $\tilde{\mu}$ is phenomenologically found to agree with g_{\dagger} in Eq. (74). The rotational velocity in Eq. (B6) found from the limiting behaviour of the MOND interpolation function thus differs from the observations of the bTFR by a factor of 4.

This paper has been typeset from a \LaTeX file prepared by the author.